Solid−Solid and Solid−Liquid Equilibria in the Heneicosane−Docosane Binary System

Valérie Metivaud, Fazil Rajabalee, Denise Mondieig,* and Yvette Haget

Centre de Physique Moléculaire Optique et Hertzienne, UMR 5798 au CNRS, Université Bordeaux I, 351 cours de la Libération, F-33405 Talence Cedex, France

Miguel Angel Cuevas-Diarte

Departament de Cristal.lografia, Mineralogia i Diposits Minerals, Facultat de Geologia, Universitat de Barcelona, C/Marti i Franquès, E−08028 Barcelona, Spain

Received July 21, 1998. Revised Manuscript Received October 9, 1998

The experimental phase diagram of the binary system implying the nonisomorphous consecutive *n*-alkanes heneicosane ($C_{21}H_{44}$) and docosane ($C_{22}H_{46}$) has been determined by combining X-ray diffraction and microcalorimetric methods. The phase diagram is very complex. X-ray experiments performed on powder samples at 288 K have shown the presence of five monophasic domains at "low temperature": three orthorhombic (Oi, Odci, and Op), one monoclinic (Mdci), and one triclinic (Tp). With increasing temperature occur successively the rotator forms RV, RI, and RII. No less than ten solid−solid and two solid−liquid biphasic domains are observed, as well as three peritectoid, one eutectoid, and one peritectic invariants. Moreover, cell parameters of mixed samples corresponding to the forms Odci (space group *Pnam*), Mdci (*Aa*), and Op ($Pca2_1$) have been determined at 288 K.

Introduction

This work, which takes part in a general study concerning the syncrystallization of substances in the alkane family, represents one part of the research done within the REALM (Réseau Européen sur les Alliages Moléculaires). Such substances are interesting from both fundamental and practical points of view. They present a rich polymorphism, the incidence of which in the formation of molecular mixed crystals is of great interest from a fundamental point of view. These kinds of materials are used in a large field of applications and they are a model for other substances, such as the polymers. Moreover, they lead to molecular alloys with important latent heat of phase transition, which are suitable MAPCM (molecular alloy phase change materials) in the field of energy storage and thermal protection.[1−4] The aim of this work is the determination of the experimental equilibrium phase diagram between two consecutive *n*-alkanes [*n*-heneicosane ($C_{21}H_{44}$) and *n*-docosane ($C_{22}H_{46}$), which will be denoted hereafter by C_{21} and C_{22}, respectively]. To our knowledge, this binary system has not been published before. However, many authors have pointed out a complex structural behavior at "low temperature" ("low temperature" is relative to the solid ordered phases) in binary systems of *n*-alkanes.[5−7] They have shown the existence of intermediate phases that do not necessarily occur in the pure components involved. Recently, Rajabalee et al.[8] assigned space groups to these forms and gave explanations concerning their occurrence in the mixed samples. These findings, added to the nonisomorphism of the two components, led us to predict a complex behavior of the binary system $C_{21} + C_{22}$. The experimental phase diagram has been determined by combining microcalorimetric and X-ray diffraction experiments.

Experimental Section

Powder X-ray Diffraction (XRD) Analyses. Crystallographic measurements at selected temperatures were made using a Siemens D500 vertical powder diffractometer. A thin plate of glass was placed between the sample to be analyzed and the sample holder to avoid the diffraction lines of copper and nickel, caused by the holder, which disturb the analyses of the diffractograms. The data were collected with a 0.05° 2θ step and 3-s interval time. Diffraction measurements were also performed versus continuous temperature variations with a Guinier−Simon camera (GS). The wavelength of copper Kα1 radiation ($\lambda = 1.5406$ Å) was used in both cases.

Calorimetric Measurements. Calorimetric measurements were carried out using a Perkin-Elmer DSC7 differential scanning calorimeter (DSC) operating in the subambient mode. Transition temperatures and enthalpies were determined from

* To whom correspondence should be addressed. Telephone: (33)556846988. Fax: (33)556846686. E-mail: dmondiei@frbdx11.cribx1.u-bordeaux.fr.

(1) Haget, Y.; Mondieig, D.; Cuevas-Diarte, M. A. CNRS Patent FR91/08695 and foreign co-pending patent applications.

(2) Mondieig, D.; Haget, Y.; Labrador, M.; Cuevas-Diarte, M. A.; Van der Linde, P. R.; Oonk, H. A. *J. Mater. Res. Bull.* **1991**, *26*, 1091.

(3) Espeau, P.; Mondieig, D.; Haget, Y.; Cuevas-Diarte, M. A. *Packag. Technol. Sci.* **1997**, *10*, 253.

(4) Mondieig, D.; Marbeuf, A.; Robles, L.; Espeau, P.; Poirier, B.; Haget, Y.; Calvet-Pallas, T.; Cuevas-Diarte, M. A. *High Temperatures-High Pressures* **1997**, *29*, 385.

(5) Luth, H.; Nyburg, S. C.; Robinson, P. M.; Scott, H. E. *Mol. Cryst. Liq. Cryst.* **1974**, *27*, 337.

(6) Gerson, A. R.; Nyburg, S. C. *Acta Crystallogr. B* **1994**, *50*, 252.

(7) Dirand, M.; Achour, Z.; Jouti, B.; Sabour, A.; Gachon, J. C. *Mol. Cryst. Liq. Cryst.* **1996**, *275*, 293.

(8) Rajabalee, F.; Metivaud, V.; Mondieig, D.; Haget, Y.; Cuevas-Diarte, M. A., accepted in *J. Mater. Res.*

10.1021/cm980737b CCC: $18.00
Published on Web 12/23/1998

four independent experiments performed on (4.0 ± 0.1)-mg samples with 2 K·min^{-1} speed of heating. Temperatures were determined from the DSC curves using the shape-factor method.[9,10] The random part of the uncertainties was estimated using the Student's method with 95% threshold of reliability.

Materials. Compounds C_{21} and C_{22} were purchased from Fluka and Aldrich, respectively, with certified purity grades of >99.5% for C_{21} and >99% for C_{22}.

The polymorphism of the two components has been studied previously in our group.[11,12] The following phase transition sequences are observed:

$$\text{Oi} \rightarrow \text{RI} \rightarrow \text{liquid for } C_{21}$$

and

$$\text{Tp} \rightarrow \text{RI} \rightarrow \text{RII} \rightarrow \text{liquid for } C_{22}$$

where Oi is orthorhombic with space group *Pcam* ($Z = 4$); T_p is triclinic ($P\bar{1}$, $Z = 1$); RI and RII, the so-called rotator forms, present an orientational disorder,[13,14] where the RI form is face-centered orthorhombic ($Fmmm$, $Z = 4$) and the RII form is hexagonal ($R\bar{3}m$, $Z = 3$).

Binary Mixed Samples. Twenty-one binary mixed samples were prepared according to the melting−quenching method; that is, the components are weighed in the desired proportions, melted, mixed to get an entirely homogeneous sample, and then quenched into liquid nitrogen.

Results and Discussion

Isotherm Characterizations. Isotherm structural characterizations versus C_{22} molar concentration were performed at 288 K and 311 K to determine the limits of monophasic and biphasic domains and the crystallographic parameters of the observed alloys.

Measurements at T = 288 K. X-ray diffraction analyses carried out on the 21 mixed samples show the presence of intermediate forms called Odci, Mdci, and Op, which do not occur in the pure components involved. In Figure 1 are represented some diffraction patterns characteristic of the different phases encountered with increasing C_{22} molar concentration. They are represented in the most pertinent 2θ-range, between 34° and 48°. The symbols ■ (Oi), ◊ (Odci), ◆ (Mdci), □ (Op), and * (Tp) are used in the diffractograms to point out some reflections specific of one particular phase that are not present in the other phases. Indexation of these reflections will be the purpose of a forthcoming paper.

The following sequence is observed with increasing C_{22} molar concentration:

$$[\text{Oi}]\rightarrow[\text{Oi} + \text{Odci}]\rightarrow[\text{Odci}]\rightarrow[\text{Odci} + \text{Mdci}]\rightarrow[\text{Mdci}]\rightarrow[\text{Mdci} + \text{Op}]\rightarrow[\text{Op}]\rightarrow[\text{Op} + \text{Tp}]\rightarrow[\text{Tp}]$$

Odci is orthorhombic ($Pnam$, $Z = 4$).[15,16] The transition between Oi and Odci is mainly characterized by the disappearance of the reflection located at $2\theta \approx 39°$ and by the increase of the intensity of the reflection at $2\theta \approx 40.5°$. Mdci is monoclinic (Aa, $Z = 4$).[16,17] The disappearance of the reflection at $2\theta \approx 41°$ together with the appearance of two reflections on the both sides of the one corresponding to $2\theta \approx 42.5°$ show the transition from Odci to Mdci. For $x = 0.05$, the reflections characterizing the Mdci form still exist. Op is orthorhombic ($Pca2_1$).[8] The Op form is mainly characterized by the occurrence of reflections located at $2\theta \approx 39.5°$ and $2\theta \approx 42.5°$. The domain [Mdci + Op] is clearly distinguished by the coexistence of two typical diffraction patterns corresponding to the Mdci and Op forms, for compositions between $x = 0.15$ and $x = 0.50$. At $x = 0.70$, reflections corresponding to the Tp form appear, whereas the ones characterizing Op decrease. At $x = 0.80$, only the Tp form remains. The Odci, Mdci, and Op forms are described in more detail elsewhere.[8,16]

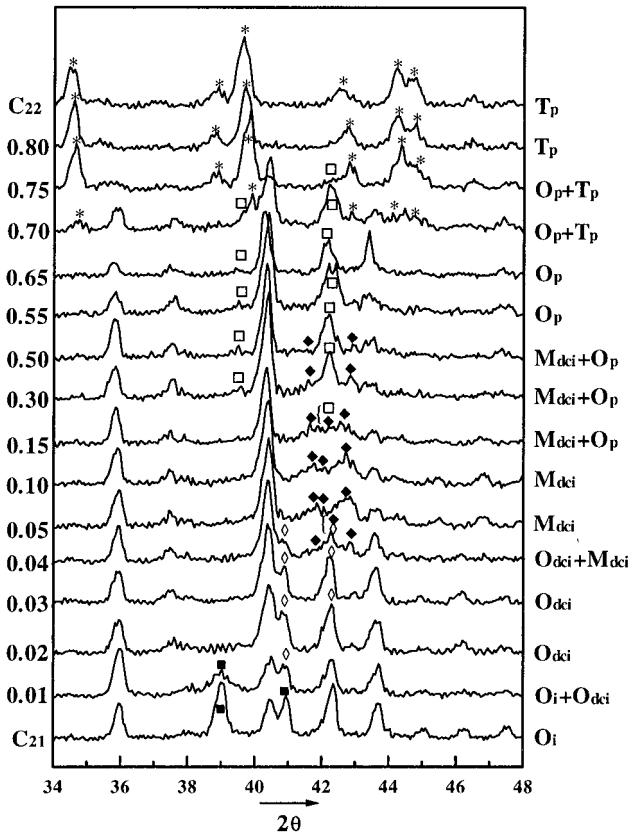

Figure 1. Isothermal structural characterization (performed at 288 K) versus C_{22} molar concentration in the range 34° ≤ 2θ ≤ 48°.

Cell Parameters of the Odci, Mdci, and Op Forms. The cell parameters of the intermediate forms Odci ($x = 0.02$), Mdci ($x = 0.05$), and Op ($x = 0.60$), which were determined at 288 K using the option "Pattern-Matching" of the program FULLPROF,[18] are given in Table 1. In addition to the determination of the cell parameters, this program allows a comparison between calculated and experimental diffraction patterns. Cell

(9) Courchinoux, R.; Chanh, N. B.; Haget, Y.; Tauler, E.; Cuevas-Diarte, M. A. *Thermochim. Acta* **1988**, *128*, 45.
(10) Courchinoux, R.; Chanh, N. B.; Haget, Y.; Calvet, T.; Estop, E.; Cuevas-Diarte, M. A. *J. Chim. Phys.* **1989**, *86(3)*, 561.
(11) Espeau, P.; Robles, L.; Mondieig, D.; Haget, Y.; Cuevas-Diarte, M. A.; Oonk, H. A. J. *J. Chim. Phys.* **1996**, *93*, 1217.
(12) Robles, L.; Mondieig, D.; Haget, Y.; Cuevas-Diarte, M. A. *J. Chim. Phys.* **1998**, *95*, 92.
(13) Sirota, E. B.; King, H. E., Jr.; Singer, D. M.; Shao, H. H. *J. Chem. Phys.* **1993**, *98(7)*, 5809.
(14) Sirota, E. B.; King, H. E., Jr.; Shao, H. H.; Singer, D. M. *J. Phys. Chem.* **1995**, *99*, 798.
(15) Nozaki, K.; Higashitani, N.; Yamamoto, T.; Hara, T. *J. Chem. Phys.* **1995**, *103(13)*, 5762.
(16) Rajabalee, F. European Label Thesis of the University Bordeaux I, France, 1998.
(17) Ungar, G. *J. Phys. Chem.* **1983**, *87*, 689.
(18) Rodriguez-Carvajal, J. *FULLPROF, a program for Rietveld refinement and pattern matching analyses*; Abstracts of the satellite meeting on powder diffraction on the XVth congress of the international Union of Crystallography, Toulouse, 1990; p 117.

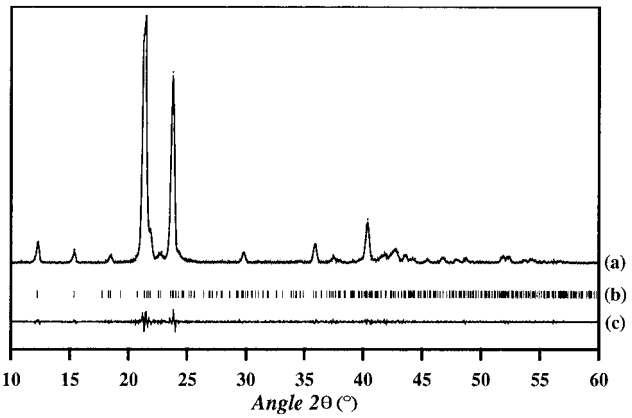

Figure 2. "Pattern-matching" analysis of the mixed sample corresponding to $x = 0.05$. (a) Experimental (crosses) and calculated (line) diffraction patterns. (b) Position of calculated reflections. (c) Difference between experimental and calculated intensities.

Table 1. Cell Parameters of Mixed Samples in the Odci, Mdci, and Op Forms Determined at 288 K

x in C_{22}	form	space group	a (Å)	b (Å)	c (Å)	β (°)
0.02	Odci	*Pnam*	7.48 (1)	4.99 (1)	57.27 (4)	90
0.05	Mdci	*Aa*	7.51 (1)	4.99 (1)	57.42 (3)	91.3 (2)
0.60	Op	$Pca2_1$	7.50 (1)	4.99 (1)	58.86 (3)	90

parameters as well as the space groups of the Odci, Mdci, and Op forms can be considered to be very reliable, as confirmed by the very good agreement between experimental and calculated diffractograms (as it is shown in Figure 2 for the mixed sample corresponding to $x = 0.05$).

Measurements at T = 311K. Representative diffraction patterns performed at 311 K are given in Figure 3. They show a large domain in composition (>80%) of RI alloys. For $x = 0.85$ and 0.90, the diffractograms exhibit two diffraction pattern families characterizing the coexistence of the RI and Tp forms. Tp alloys are observed for compositions very close to C_{22}.

Isopleth Characterizations. *Central Composition.* The X-ray analysis by the GS chamber carried out on the mixed sample $C_{21}(0.5)+C_{22}(0.5)$ (Figure 4) points out the following sequence with increasing temperature:

$$[\text{Mdci} + \text{Op}]\rightarrow[\text{Op} + \text{RV}]\rightarrow[\text{RV}]\rightarrow[\text{RI}]\rightarrow[\text{RI} + \text{RII}]\rightarrow[\text{RII}]\rightarrow[\text{RII} + \text{L}]\rightarrow[\text{L}]$$

The nature of the "low temperature" form is hardly distinguishable in this photograph. However, isothermal X-ray measurements performed at 288 K allow us to assert that the mixed sample is biphasic [Mdci + Op]. The RV form, which is only observed by cooling of C_{22}, appears before the RI form in the mixed samples. The [RV]→[RI] transition is of second order. The transition from the ordered to the rotator form RV is characterized by the disappearance of many reflections due both to the disorder and to the fact that the symmetry of the molecule increases. The RI form, which shows a rotational disorder of the molecule along its *c* long axis, is very much affected by temperature. The disorder strongly increases with temperature. This fact is reflected in the GS photograph by a clear evolution of the reflections (111) and (020) with increasing temperature. These two reflections come to a single one (101) synonymous with

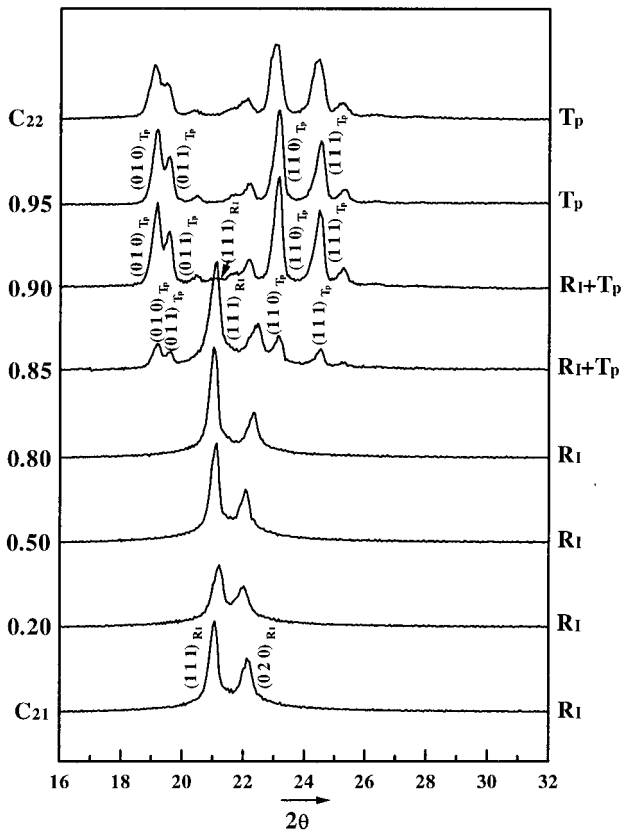

Figure 3. Isothermal structural characterization (performed at 311 K) versus C_{22} molar concentration in the range $16° \leq 2\theta \leq 32°$.

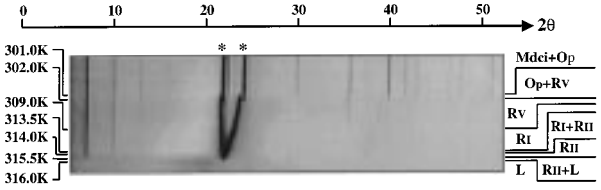

Figure 4. Guinier−Simon photograph of the mixed sample $C_{21}(0.5)+C_{22}(0.5)$ performed between 293 K and 319 K [the two reflections indicated by an asterisk correspond to the reflections (110) and (020) at "low temperature", which come to (111) and (020) in the RV and RI forms to reach (010) in the RII form].

the passage to the hexagonal RII form. The biphasic domains observed are very narrow.

Compositions Rich in C_{21}. Due to the narrowness of the Oi and Odci domains (as it was shown in the isotherm characterization at 288 K), many X-ray studies, combined with calorimetric experiments, were carried out with increasing temperature in order to determine the experimental phase diagram in the region close to C_{21}. As an example, the more representative diffractograms performed on the mixed sample corresponding to $x = 0.03$ are given in Figure 5.

The sequence [Odci]→[Odci + Mdci]→[Mdci]→[RV] is observed with increasing temperature. The entrance into the biphasic domain [Odci + Mdci] is observed at 300.5 K by the decrease of reflections corresponding to $2\theta \approx 41°$ and $2\theta \approx 42°$, whereas two reflections appear on both sides of the one corresponding to $2\theta \approx 42°$ (which are clearly visible at 301.5 K). At 302.5 K, the reflections characterizing the Mdci form remain. At $T = 303.5$ K, the sample is monophasic RV. The biphasic

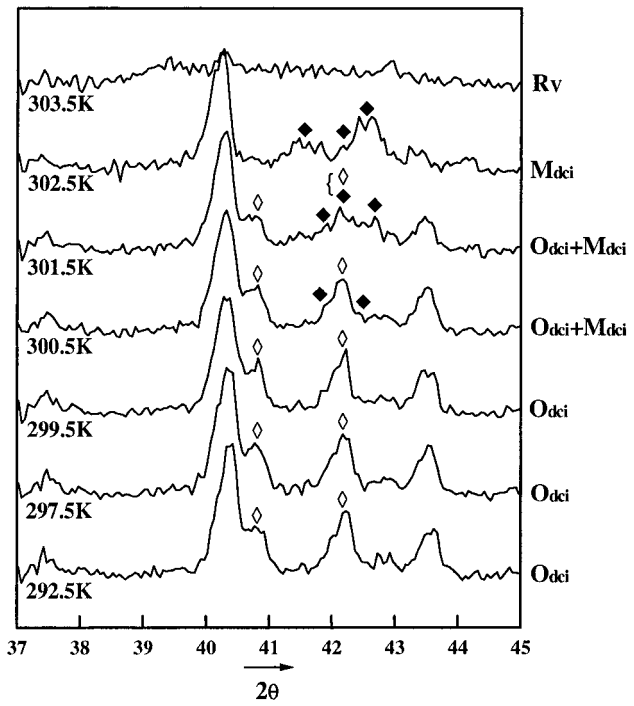

Figure 5. X-ray diffraction patterns performed between 292.5 K and 303.5 K on the composition corresponding to $x = 0.03$ (range $37° \leq 2\theta \leq 45°$). The main reflections characterizing the Odci and Mdci forms are represented by the symbols ◊ and ◆, respectively.

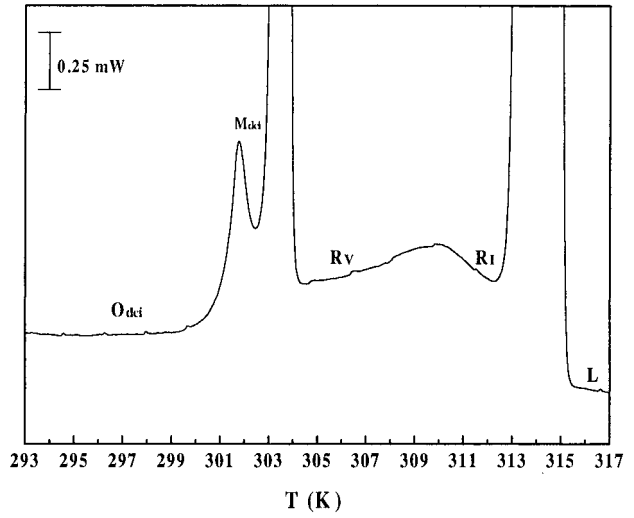

Figure 6. DSC curve of the mixed sample corresponding to $x = 0.03$ between 298 K and 317 K.

domain [Mdci + RV] was not observed because of its extreme narrowness. The same sequence was observed by calorimetric measurements. The amplification of the DSC curve of the sample corresponding to $x = 0.03$ is given in Figure 6. This figure points out the existence of first-order transitions [Odci]→[Mdci] and [Mdci]→[RV] at "low temperature".

The "low temperature" experimental phase diagram in the area close to C_{21} (for $0 \leq x \leq 0.10$) is represented in Figure 7 together with the results of X-ray experiments and experimental points determined from the DSC curves. Figure 7 points out the presence of two peritectoid invariants located, according to X-ray data, at $T_{p_1} \approx 303.5$ K and $T_{p_2} \approx 303.2$ K.

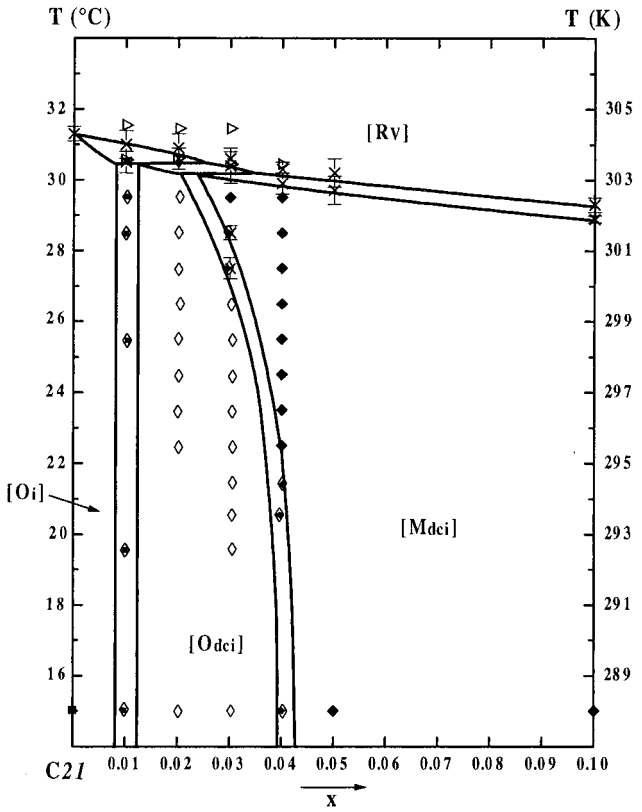

Figure 7. "Low temperature" part of the phase diagram $C_{21} + C_{22}$ in the area close to ($0 \leq x \leq 0.10$) deduced from DSC experiments (×) and X-ray measurements (the symbols ■, ◊, ◆, and "tilted triangle" represent the domains of mixed samples with Oi, Odci, Mdci, and RV structures, respectively; biphasic domains are represented with the two symbols corresponding to the forms involved.

Compositions Rich in C_{22}. For the composition $x = 0.75$, starting from 288 K, the following sequence is observed with increasing temperature (Figure 8).

$$[Op + Tp] \rightarrow [Tp + RV] \rightarrow [RV]$$

Diffractograms performed at 303 K and 304 K are clearly distinguished by the coexistence of two typical patterns, characterizing the Tp and Op forms in the first case and the Tp and RV forms in the second case. The direct passage from [Op + Tp] to [Tp + RV] points out the existence of a peritectoid invariant located between 303 K and 304 K. The coexistence between Tp and RV remains until 307 K. At 308 K, the sample is monophasic RV.

Energetic Characterization. Calorimetric measurements performed on 19 binary mixed samples allowed the determination of transition temperatures and enthalpies. Figure 9 shows the DSC curves between 293 K and 323 K. This set of curves clearly reveals the presence of a eutectoid invariant located at $T_{E_1} = (300.8 \pm 0.2)$ K. The two intense peaks observed for each composition are relative to the transitions "low temperature" ordered form→R (V or I) and R (I or II)→liquid, respectively. The weak peak appearing just before the melting one for compositions between $x = 0.20$ and $x = 0.95$ corresponds to the RI→RII transition. The second-order transition RV→RI is only observable in an amplifying scale (see Figure 6). "Low temperature" energetic parameters (i.e., transition temperatures and

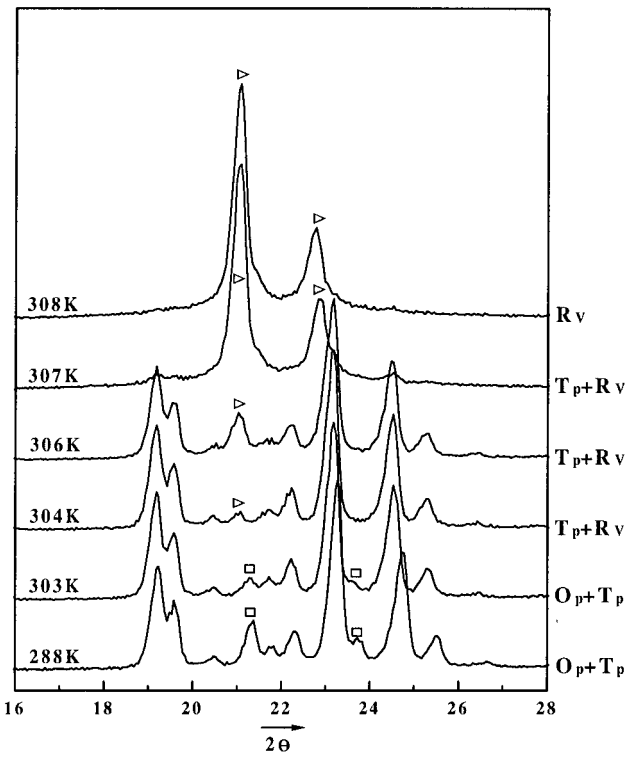

Figure 8. X-ray diffraction patterns (range $16° \leq 2\theta \leq 28°$) of the mixed sample corresponding to $x = 0.75$ performed between 288 K and 308 K. The reflections characterizing the Op and RV forms are represented by the symbols □ and "tilted triangle", respectively, the other reflections are characteristic of the Tp form.

enthalpies between a solid ordered form and a rotator form) are given in Table 2. T_{p_3} corresponds to the temperature of the peritectoid invariant, which was pointed out by X-ray experiments. Energetic characteristics corresponding to transitions between rotator forms and to the melting are reported in Table 3.

Experimental Phase Diagram. The binary phase diagram of $C_{21} + C_{22}$, determined by the calorimetric and X-ray experiments, is presented in Figure 10, together with the most representative X-ray data determined at 288 K and 311 K. The diagram is characterized by the following parameters:

nine monophasic domains: [Oi], [Odci], [Mdci], [Op], [Tp], [RV], [RI], [RII], and [L]

ten solid−solid domains: [Oi + Odci], [Odci + Mdci], [Mdci + Op], [Op + Tp], [Oi + RV], [Odci + RV], [Mdci + RV], [Op + RV], [Tp + RV] and [RI + RII]

two solid−liquid domains: [RI+L] and [RII+L]

three peritectoid invariants located at $T_{p_1} \approx 303.5$ K between $x \approx 0.005$ and $x \approx 0.025$, $T_{p_2} \approx 303.2$ K between $x \approx 0.020$ and $x \approx 0.035$, and $T_{p_3} \approx 303.8$ K between $x \approx 0.69$ and $x \approx 0.77$

one eutectoid invariant located at $T_{E_1} \approx 300.8$ K between $x \approx 0.22$ and $x \approx 0.52$ and

one peritectic invariant located at $T_{p_4} \approx 314.0$ K between $x \approx 0.02$ and $x \approx 0.11$.

Conclusion

The structural behavior of the binary phase diagram $C_{21} + C_{22}$ is very complex, both at "low" and "high" temperatures. No less than three "low temperature" phases, which do not occur in the pure components C_{21} and C_{22}, are observed: they are, one monoclinic (Mdci) and two orthorhombic (Odci and Op) ones. These forms are induced by conformational defects.[8,16]

Previous studies performed on numerous other binary systems of *n*-alkanes (from C_{16} to C_{28})[16] have shown that

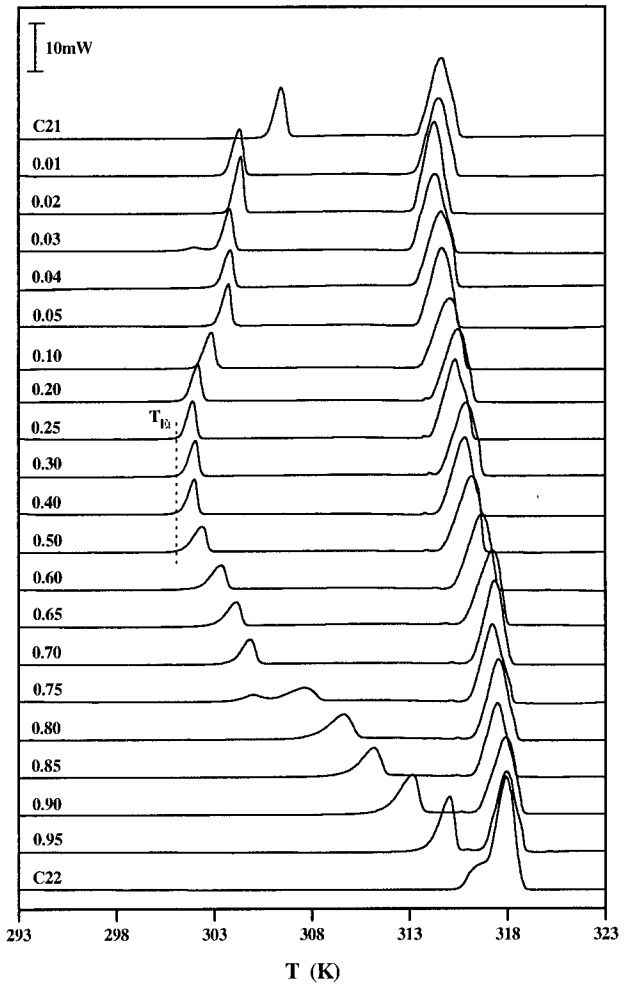

Figure 9. Evolution of the DSC curves as a function of molar fraction in C_{22} and temperature.

Table 2. Temperature and Enthalpy Parameters of the Solid Ordered Phase → Rotator Phase Transitions[a]

	solid ordered phase → R				
x	T_{solvi}	T_E	T_{p_3}	T_{solvs}	ΔH_m
0.00				304.3 ± 0.2	15.7 ± 0.6
0.01	303.5 ± 0.3			304.0 ± 0.4	14.3 ± 0.6
0.02	303.6 ± 0.3			303.9 ± 0.4	13.9 ± 0.1
0.03	303.4 ± 0.5			303.6 ± 0.2	12.1 ± 0.6
0.04	302.9 ± 0.3			303.3 ± 0.2	11.4 ± 0.5
0.05	302.7 ± 0.4			303.2 ± 0.4	10.8 ± 0.1
0.10	301.9 ± 0.1			302.3 ± 0.2	10.7 ± 0.3
0.20	301.2 ± 0.2			301.7 ± 0.2	10.3 ± 0.1
0.25		300.8 ± 0.2		301.3 ± 0.3	10.1 ± 0.5
0.30		300.8 ± 0.2		300.9 ± 0.3	9.9 ± 0.3
0.40		300.8 ± 0.1		301.4 ± 0.2	10.3 ± 0.1
0.50		301.0 ± 0.1		301.8 ± 0.2	10.2 ± 0.2
0.60	301.6 ± 0.2			302.8 ± 0.1	10.4 ± 0.2
0.65	302.3 ± 0.1			303.5 ± 0.5	10.5 ± 0.1
0.70	303.2 ± 0.3			304.1 ± 0.4	10.4 ± 0.6
0.75			303.8 ± 0.2	307.3 ± 0.3	13.2 ± 0.3
0.80	306.0 ± 0.2			309.4 ± 0.3	16.0 ± 0.6
0.85	308.6 ± 0.3			311.0 ± 0.2	18.2 ± 0.4
0.90	310.2 ± 0.3			312.9 ± 0.5	22.3 ± 0.6
0.95	312.9 ± 0.3			314.5 ± 0.5	23.6 ± 0.8
1.00				316.0 ± 0.2	27.3 ± 1.6

[a] Temperatures are in K and enthalpies in $kJ \cdot mol^{-1}$.

Table 3. Thermo-energetic Parameters Relative to Transitions between Rotator Phases and Melting[a]

	RV→RI	RI→RII		RI→L		
x	T	T_{solvi}	T_{solvs}	T_{sol}	T_{liq}	ΔH_m
0.00					312.8 ± 0.2	46.9 ± 1.0
0.01	310.7 ± 0.4			313.3 ± 0.2	313.5 ± 0.2	46.2 ± 0.9
0.02	310.7 ± 0.2			313.4 ± 0.3	313.6 ± 0.4	45.9 ± 0.1
0.03	310.9 ± 0.3			313.7 ± 0.3	314.0 ± 0.1	45.8 ± 0.6
0.04	310.9 ± 0.4			313.5 ± 0.1	313.7 ± 0.2	45.9 ± 0.5
0.05	310.5 ± 0.4			313.6 ± 0.2	313.8 ± 0.4	45.8 ± 2.0
					RII→L	
0.10	310.1 ± 0.1			313.6 ± 0.2	313.9 ± 0.3	45.7 ± 0.8
0.20	309.9 ± 0.1	313.4 ± 0.2	313.5 ± 0.1	314.0 ± 0.1	314.4 ± 0.2	45.8 ± 0.9
0.25	310.2 ± 0.2	313.4 ± 0.2	313.5 ± 0.2	314.2 ± 0.1	314.7 ± 0.3	45.9 ± 0.5
0.30	309.5 ± 0.1	313.5 ± 0.2	313.6 ± 0.2	314.5 ± 0.1	314.9 ± 0.1	46.0 ± 1.0
0.40	309.8 ± 0.1	313.6 ± 0.1	313.7 ± 0.1	315.0 ± 0.1	315.4 ± 0.1	46.2 ± 0.3
0.50	309.8 ± 0.3	313.8 ± 0.1	313.9 ± 0.1	315.3 ± 0.2	315.8 ± 0.2	46.6 ± 0.6
0.60	310.2 ± 0.1	314.1 ± 0.1	314.2 ± 0.1	315.7 ± 0.1	316.1 ± 0.2	47.0 ± 0.3
0.65	310.6 ± 0.4	314.3 ± 0.1	314.5 ± 0.1	315.9 ± 0.2	316.2 ± 0.2	47.1 ± 0.9
0.70	310.6 ± 0.3	314.5 ± 0.3	314.7 ± 0.2	316.1 ± 0.4	316.3 ± 0.3	47.5 ± 0.9
0.75	310.7 ± 0.6	314.7 ± 0.3	314.9 ± 0.2	316.2 ± 0.3	316.4 ± 0.3	47.8 ± 0.9
0.80	311.5 ± 0.7	315.1 ± 0.2	315.2 ± 0.2	316.3 ± 0.1	316.5 ± 0.2	48.0 ± 0.3
0.85		315.3 ± 0.2	315.4 ± 0.2	316.4 ± 0.2	316.5 ± 0.3	48.1 ± 0.4
0.90		315.5 ± 0.3	315.6 ± 0.3	316.4 ± 0.4	316.6 ± 0.3	48.4 ± 1.0
0.95		315.6 ± 0.2	315.7 ± 0.2	316.6 ± 0.3	316.8 ± 0.4	48.7 ± 0.8
1.00			316.1 ± 0.2		316.7 ± 0.2	49.1 ± 1.2

[a] Temperatures are in K and enthalpies in kJ·mol^{-1}.

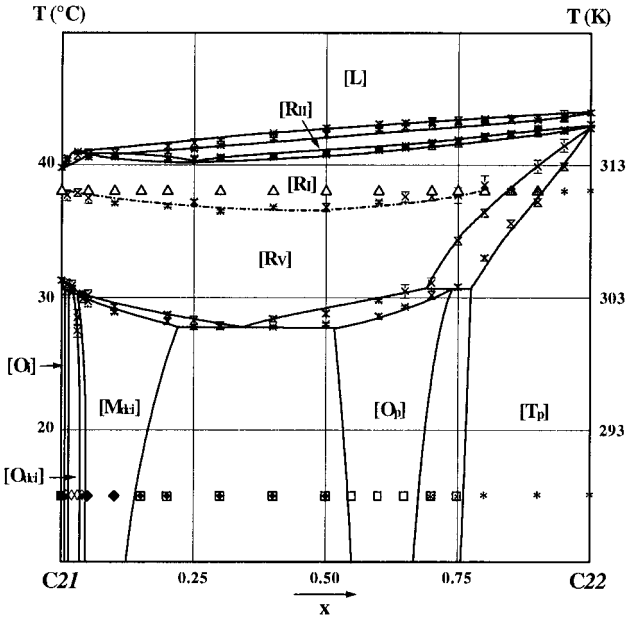

Figure 10. Experimental phase diagram of the binary system $C_{21}H_{44}$−$C_{22}H_{46}$. Results of X-ray measurements performed at 288 K and 311 K are represented by the symbols ■ (Oi), ◊ (Odci), ◆ (Mdci), □ (Op), and * (Tp). Biphasic domains are represented with the two symbols corresponding to the forms involved.

the Mdci form always appears in all the systems, implying at least one odd alkane in the composition range(s) close to the odd alkane(s).

The Odci form, which is stable in *n*-alkanes of higher chain lengths (from C_{23} and at least till C_{29}),[19] occurs for the first time in the system C_{19} + C_{20} (subject of another paper) and continues to Oi. Its domain is very narrow. When Odci is stable in none of the two components involved, it is always observed close to the odd alkane but appears only if the odd alkane has the shortest chain length. Then, for example, it is not encountered in the system C_{20} + C_{21} where the odd alkane has the highest chain length.

The Op form is always encountered close to the Tp form in systems, implying at least one even alkane and in the central part of odd−odd systems, excepting the C_{25} + C_{27} one, in which the miscibility in the Mdci form is total.

In the system C_{21} + C_{22}, the extent in the composition range of each "low temperature" monophasic domain is narrow, whereas very large domains of the rotator forms RV and RII occur at "high temperature". The miscibility is total in the RI phase. RV, which is only observed in pure C_{22} on cooling, is stabilized in the mixtures of C_{21} + C_{22}. Our previous studies[16] have shown that this form, which always precede the RI one with increasing temperature, is observed in all the systems that exhibit a RII form before melting: it is never observed in systems with smaller number of carbon atoms (Cn_1−Cn_2 with n_1 and $n_2 \leq 21$), in which the only stable rotator form is the RI one.

To conclude, it can be said that the mixing stabilizes the disordered forms, both at "low" (phases presenting conformational defects) and "high" (rotator phases) temperatures. Moreover, from a practical point of view, the high values of enthalpies of melting, combined with narrow thermal windows (temperature difference between liquidus and solidus), enable us to say that C_{21} + C_{22} mixtures can be good candidates for the storage of energy and the thermal protection.

CM980737B

(19) Snyder, R. G.; Maroncelli, M.; Qi, S. P.; Strauss, H. L. *Science* **1981**, *214*, 188.